

Stiffening of organosilicate glasses by organic cross-linking

Han Li^{a,1}, Jan M. Knaup^{b,c}, Efthimios Kaxiras^{a,b,c}, Joost J. Vlassak^{a,*}

^a School of Engineering and Applied Sciences, Harvard University, Cambridge, MA 02138, USA

^b Department of Physics, Harvard University, Cambridge, MA 02138, USA

^c Ecole Polytechnique Fédérale de Lausanne, Station 12, CH-1015 Lausanne, Switzerland

Received 26 April 2010; received in revised form 21 July 2010; accepted 12 August 2010

Available online 15 October 2010

Abstract

Atomistic simulations show that organosilicates, used as low permittivity dielectric materials in advanced integrated circuits, can be made substantially stiffer than amorphous silica, while maintaining a lower mass density. The enhanced stiffness is achieved by incorporating organic cross-links to replace bridging oxygen atoms in the silica network. To elucidate the mechanism responsible for the enhanced stiffness, the conformational changes in the network upon hydrostatic and shear loading are examined. The structural and mechanical impact of terminal methyl groups is also assessed quantitatively and compared with continuous random network theory. © 2010 Acta Materialia Inc. Published by Elsevier Ltd. All rights reserved.

Keywords: Low k dielectrics; Amorphous; Elastic properties; Molecular-dynamics simulation

1. Introduction

Continued miniaturization of integrated circuits requires interconnect insulator materials with reduced dielectric constant (k) [1–3]. Organosilicate glasses (OSG) are a family of organic–inorganic hybrid materials that possess a silica-like backbone structure with k values typically in the range 2.7–3, compared with 3.9–4 for silica. Already implemented in the 90 nm and 65 nm nodes [4,5], OSG-type materials are also widely regarded as the most promising low k dielectrics for future integrated circuit technologies. The low dielectric constant is achieved by introducing organic terminal groups into the silica network. This modification decreases the OSG density and lowers the bond polarizability, both beneficial for the dielectric performance. The dielectric constant is reduced even further by making the OSG porous. From a mechanical point of view, the terminal groups disrupt the glass net-

work and degrade the mechanical integrity of the materials. Successful integration into integrated circuits of OSG with high porosity levels imposes stringent demands on the mechanical properties of the OSG to better withstand the rigors of the fabrication process.

The mechanical properties of amorphous solids are determined essentially by their covalent network structure [6–11]. Experiments have demonstrated that the elastic modulus and fracture toughness of as-deposited OSG thin films can be improved by broadband ultraviolet (UV) irradiation and thermal treatment [7,8,10]. Such improvements are associated with a more densely cross-linked network structure attained by removing terminal groups and by forming networking bonds [8,10,12]. The same principle can also be used to strengthen films during film deposition: by engineering the precursor monomers and synthesis conditions, hydrocarbon molecules can be incorporated into the material matrix as network-forming units rather than as terminal groups, resulting in a network that is less disrupted and has improved strength [9,11,13,14]. To better understand this strengthening mechanism, quantitative molecular modeling is indispensable.

Using constraint theory, amorphous solids have been modeled as continuous random networks [6,15]. Each atom

* Corresponding author.

E-mail address: vlassak@esag.harvard.edu (J.J. Vlassak).

¹ Present address: IBM Thomas J. Watson Research Center, Yorktown Heights, NY 10598, USA.

in the network is covalently bonded to its nearest neighbors, and subject to constraints associated with bond stretching and bending. In such networks all bonds are viewed as equivalent and the network is quantified by the average coordination number of all network-forming atoms, termed the network connectivity $\langle r \rangle$. He and Thorpe [15] have shown by means of numerical simulations that the elastic properties of random networks are determined by their network connectivity value. Rigidity percolation occurs and the system transforms from floppy (under-constrained) to stiff (over-constrained) as the connectivity number exceeds a threshold value $\langle r \rangle_c$. The constraint theory argument, however, may not be directly applicable to complex materials such as organosilicates, where different covalent bonds and non-bond interactions also need to be accounted for. To this end, atomistic models with sophisticated interatomic potentials have been developed [16–18]. A popular approach to constructing models for OSG-like materials consists of modifying the backbone structure of amorphous silica [19–22]. Molecular dynamics (MD) simulations using these atomistic models have been able to reproduce experimental observations to a certain extent [19–22], but a fundamental mechanistic understanding of the structure–property relationships is still lacking. Further studies are needed to develop the critical insight required to guide material developments.

The objective of this paper is to focus on dense OSG materials and to systematically and quantitatively explore how their mass density and mechanical properties are correlated with the network structure. To delineate the respective roles of various bridging and terminal groups, two classes of OSG models are considered. The first class of models consist of Si–O–Si and Si–CH₂–Si networks without terminal groups, referred to as type-I OSG models. The second class of models, type-II OSG models, have only Si–O–Si bonds in the network, but terminal groups (–OH or –CH₃) are allowed. We demonstrate the potential of synthesizing stiffer than silica OSG-type materials by organic cross-linking and by limiting the terminal group population. To elucidate the mechanism of enhanced stiffness, network deformation upon hydrostatic and shear loading is analyzed. The implications for developing porous ultralow k dielectrics with improved mechanical properties are discussed.

2. Model construction

Construction of the OSG models involves two major steps, as illustrated in Fig. 1. The starting structure consists of a 64 atom amorphous silicon model generated previously by slow quenching of liquid silicon followed by a sim-

ulated anneal [16]. The interatomic potential used for this simulation accounts for the dependence of chemical bonding (bond order, hybridization, and so forth) on the local coordination number, and has been demonstrated to generate realistic amorphous silicon structures [16].

In step 1 the amorphous silicon supercell (Fig. 2a) is first expanded in all three dimensions by a factor of 1.338 to ensure that the derivative silica model will have a density of 2.2 g cm^{−3} before structural relaxation. After expansion all Si–Si pairs are replaced by Si–O–Si. The Si–O–Si bond angle is initially set at 150° with a random orientation about the former Si–Si bonds. The resultant silica structure (Fig. 2b) is then relaxed by potential energy minimization. More details on the interatomic potential used in this study for the relaxation and MD simulations are provided below. The supercell is allowed to change shape and size without any structural constraints other than periodic boundary conditions in the three directions.

In step 2 we derive type-I and type-II OSG models based on the relaxed amorphous silica (a-silica) model using the following procedure. For type-I models a fraction of the bridging oxygen atoms in the silica backbone structure are replaced by methylene groups (Fig. 2c), such that the network connectivity remains unchanged compared with silica (the methylene group is regarded as one “atom”). For type-II models a number of Si–O–Si units in the silica structure are converted into pairs of Si–T units by breaking the Si–O bonds and replacing the oxygen atom with two T groups, where T denotes a terminal group that can be either –OH or –CH₃. The selection of terminal groups is guided by experimentation [8,23,24]. These terminal groups are randomly oriented, provided no overlap between atoms occurs. Before carrying out the MD simulations the structures are relaxed by potential energy minimization (Fig. 2d). For statistical purposes, five configurations in which terminal positions are randomly selected are constructed for each composition. Preliminary simulations using OSG models that were eight times as large indicate that finite size effects are insignificant for the properties investigated in this study. The results presented in this paper by default refer to the 64 Si atom models unless otherwise specified.

3. Simulation protocol

The MD simulations were performed using the COMPASS force field [25]. COMPASS is an empirical many-body potential that has been extensively parameterized using ab initio calculations and experimental data, with a functional form that includes covalent terms as well as long-range, non-bond interactions (i.e. van der Waals and electrostatic forces).

The MD simulations in this study consist of two sequential steps: equilibration and property sampling. A typical equilibration starts with 20 ps of NVT dynamics during which volume and temperature are kept constant, followed by NPT dynamics during which pressure and temperature



Fig. 1. Flowchart for generating the type-I and type-II OSG models.

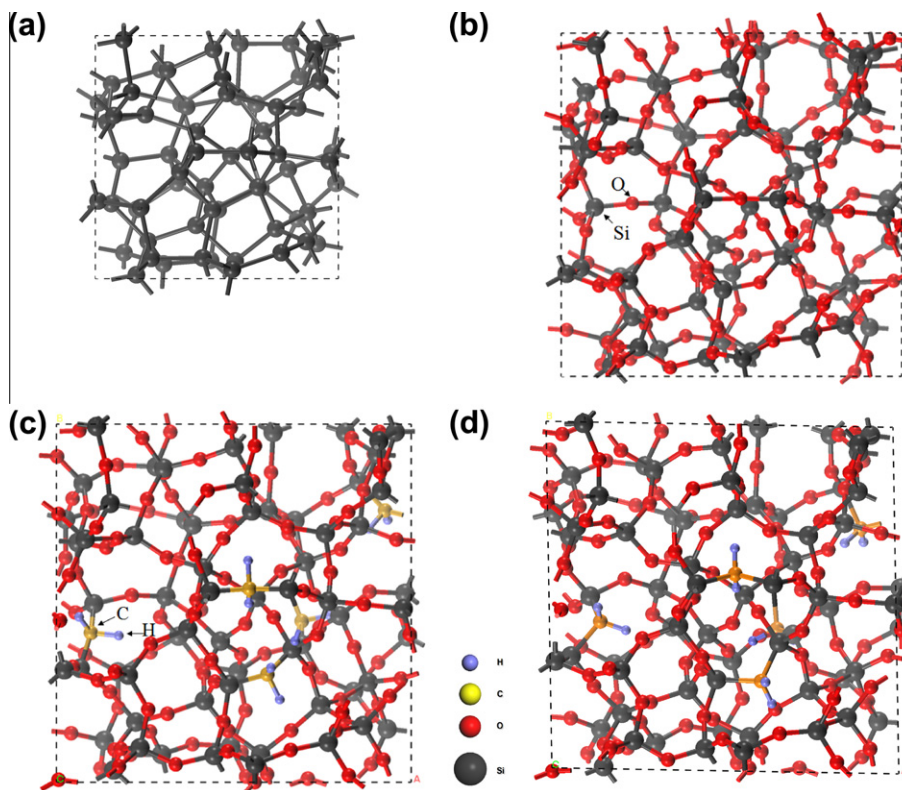


Fig. 2. Unit cell of (a) amorphous silicon with 64 Si atoms, (b) silica derived from (a), (c) type-I OSG with five methylene cross-links and (d) relaxed OSG from (c).

are maintained constant. Preliminary simulations showed that the 20 ps NVT step prevents incidental trajectory divergence in the subsequent NPT simulation. Similar procedures have been used by other researchers [26]. The NPT step continues until the energy and temperature of the system reach a steady state for more than 100 ps, and lasts from 200 to 1600 ps depending on the model. System temperature is maintained at 298 K using Andersen's thermostat [27]. In the NPT ensemble the external stress is controlled by the Parrinello–Rahman method [28]. Hydrostatic pressures and shear stresses are applied to the OSG supercell to simulate volumetric and shear deformation, respectively. After equilibration the NPT simulation is continued for another 20 ps to generate trajectories to be used in extracting time-averaged structural and mechanical properties. The complete 6×6 elastic stiffness matrix can be obtained following a standard procedure [29]. The bulk modulus and shear modulus are calculated from the elastic constants using [29]:

$$B = (C_{11} + C_{22} + C_{33} + 2C_{12} + 2C_{13} + 2C_{23})/9 \quad (1)$$

$$G = (C_{11} + C_{22} + C_{33} + 2C_{44} + 2C_{55} + 2C_{66} - C_{12} - C_{13} - C_{23})/15 \quad (2)$$

In all simulations periodic boundary conditions are imposed in all three directions. Electrostatic potential summation is conducted using Ewald's method [30] with a cut-off distance of 12.5 Å. The velocity-Verlet algorithm based on the original Verlet algorithm [31] is used to integrate New-

ton's equations of motion with a time step of 1 fs. Extensive preliminary simulations were conducted to ensure that the structure was sufficiently equilibrated and convergent results were obtained under the specified conditions. The simulations were performed using the software package Materials Studio [32].

4. Results and discussion

4.1. Type-I OSG: effect of organic bridging units

4.1.1. Structural and elastic properties at zero pressure

Our simulation results show that the incorporation of $-\text{CH}_2-$ as cross-links in the silica network has a pronounced impact on the structure and mechanical properties of the resultant organosilicates. For the a-silica model the calculated mass density and the Si–O–Si angle distribution agree well with experimental measurements on silica glasses [33–35]. The O–Si–O angle exhibits a tight distribution with a maximum at 109.4° , indicating nearly perfect SiO_4 tetrahedra. As the silica network is chemically modified the density of type-I OSG first increases slightly and then decreases rather quickly with further $-\text{CH}_2-$ introduction (Fig. 3a). The overall trend is in reasonable agreement with predictions from density functional theory based on the tight binding (DFTB) method [36]. Evidently, the introduction of methylene cross-links reduces the material density significantly. Note that the density results calculated using

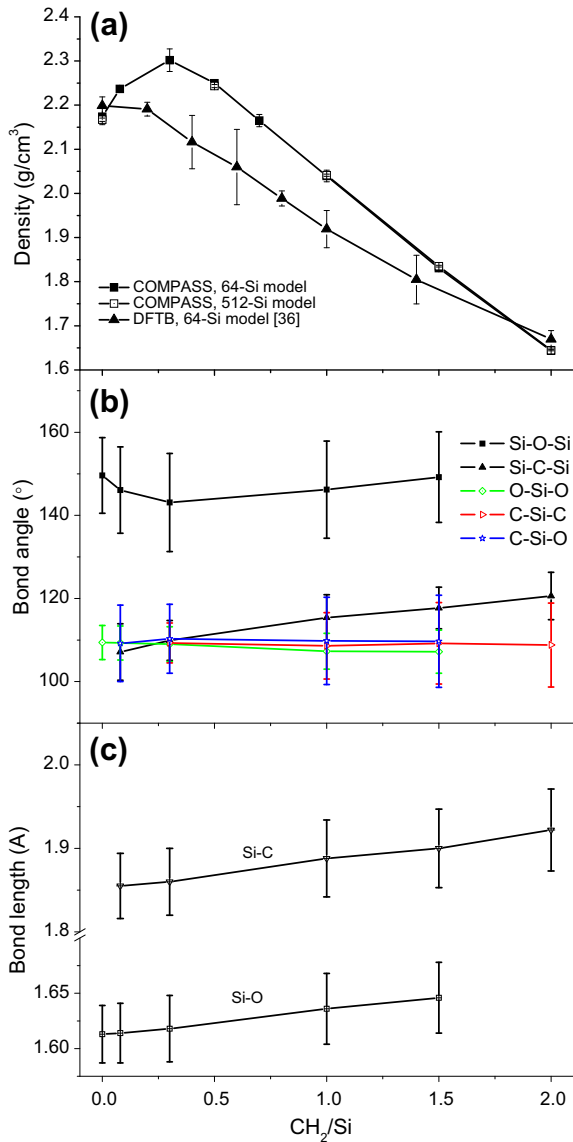


Fig. 3. (a) Mass density of type-I OSG, (b) various bond angles and (c) bond length as a function of CH_2/Si ratio. The error bars denote one standard variation.

models eight times as large closely overlap with the results for the smaller OSG models, indicating that the finite size does not affect the density calculations significantly.

The change in material density is due to (1) the CH_2 group being 12.5% lighter than an oxygen atom and (2) the evolution of the various bond lengths and angles as the silica structure is modified (Fig. 3b and c). The Si–O–Si and Si–C–Si bonds are relatively flexible in bending and, hence, are most sensitive to changes in the composition. In contrast, the O–Si–O, C–Si–C and C–Si–O bonds within the individual silicon tetrahedral units are very stiff and the corresponding bond angles remain essentially unchanged. A closer look reveals that the mean Si–C–Si angle increases monotonically as the $-\text{CH}_2-$ concentration increases (Fig. 3b). The same holds true for the Si–O and Si–C bond lengths (Fig. 3c), although the relative varia-

tions are much smaller. These structural changes expand and open up the network, thus reducing the density. The mean Si–O–Si bond angle goes through a minimum with increasing $-\text{CH}_2-$ population (Fig. 3b); this minimum corresponds to the OSG composition with the greatest density ($\text{CH}_2/\text{Si} \approx 0.3$). When $-\text{CH}_2-$ is dilute in the network the decrease in Si–O–Si angle counteracts the effect of the Si–C–Si, Si–C and Si–O bonds; after reaching the composition of minimum Si–O–Si angle, all structural changes act to reduce the material density. Therefore, the glass network enlarges more effectively, leading to a fast decrease in density with increasing $-\text{CH}_2-$ population.

Introducing $-\text{CH}_2-$ groups as bridging units changes the elastic properties of the OSG. Indeed, the bulk modulus gradually increases from the value of pure silica (~ 39.5 GPa) to 59.3 GPa as half of the oxygen atoms are replaced (see Fig. 4a). Further increasing the $-\text{CH}_2-$ content continues the trend, but at a lower rate; an additional enhancement of only 16% can be obtained when the remaining oxygen atoms are completely substituted by $-\text{CH}_2-$ groups. Calculations using DFTB reproduce a similar trend for the bulk modulus [36]. In contrast, the shear modulus of the OSG model depends only slightly on the $-\text{CH}_2-$ population, without significant change from the silica value, as shown in Fig. 4a. Fig. 4b plots Young's modulus of type-I OSG as a function of the CH_2/Si ratio, along

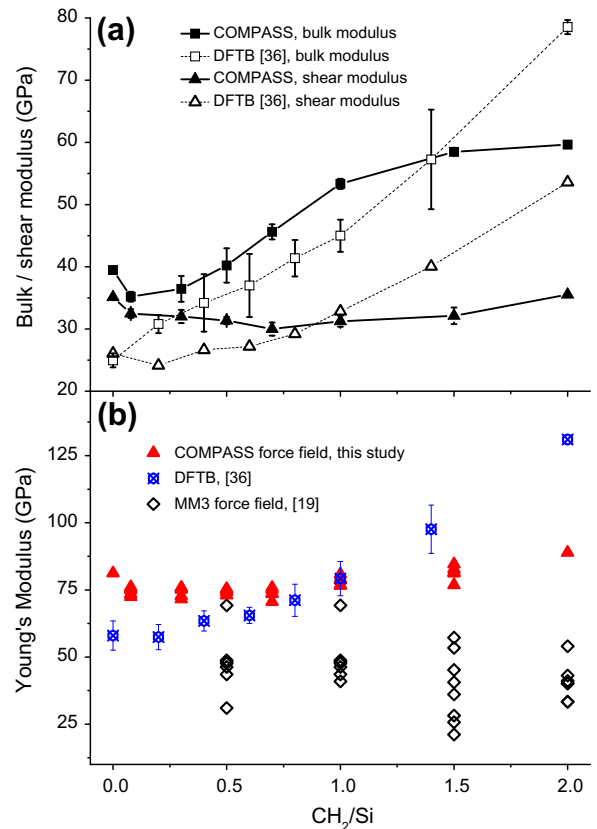


Fig. 4. (a) Bulk modulus and shear modulus and (b) Young's modulus of type-I OSG as a function of CH_2/Si ratio for different potentials.

with results obtained using DFTB [36] and the MM3 force field [19]. Evidently, our results are consistent with the calculation from density function theory, although a more significant increase in elastic modulus (bulk, shear and Young's modulus) is obtained for the latter. The increased stiffness with $-\text{CH}_2-$ concentration is caused by the higher bending rigidity of Si–C–Si bonds than that of Si–O–Si bonds, and will be explained further in Section 4.1.2. Comparison with the results in Tajima et al. [19] is difficult, primarily because of the large scatter in the modulus values reported in this reference; no clear trend can be discerned. In general, we note that heavily distorted models or models that are insufficiently relaxed can give rise to much reduced modulus values. This reduction in stiffness has been attributed to the fact that the network bond configuration is energetically less stable than well-relaxed models and thus more easily deformed [8,10].

While the observation that the mechanical behavior of OSG is sensitive to the precise network structure is well known from experiments [7,8,37], the finding that it may

be possible to produce OSG materials that are less dense but substantially stiffer than silica is somewhat unexpected. The increased stiffness contrasts with the commonly held perception that organic cross-linking renders the network more compliant.

4.1.2. Bond deformation under hydrostatic and shear loading

To better understand the elastic properties of type-I OSG and in particular the mechanism responsible for the enhanced stiffness, all possible bond stretching and bending molecular deformation modes are investigated under hydrostatic and pure shear loading conditions. For simplicity, we focus our discussion on the materials at either end of the composition spectrum, i.e. SiO_2 and $\text{Si}(\text{CH}_2)_2$.

Evolution of the SiO_2 network structure under hydrostatic pressures is documented in the left panels of Fig. 5. It is evident from the plots that the bulk deformation of SiO_2 is mostly associated with a change in the Si–O–Si bond angle distribution. In comparison, the distributions of the Si–O bond length and the O–Si–O angle remain

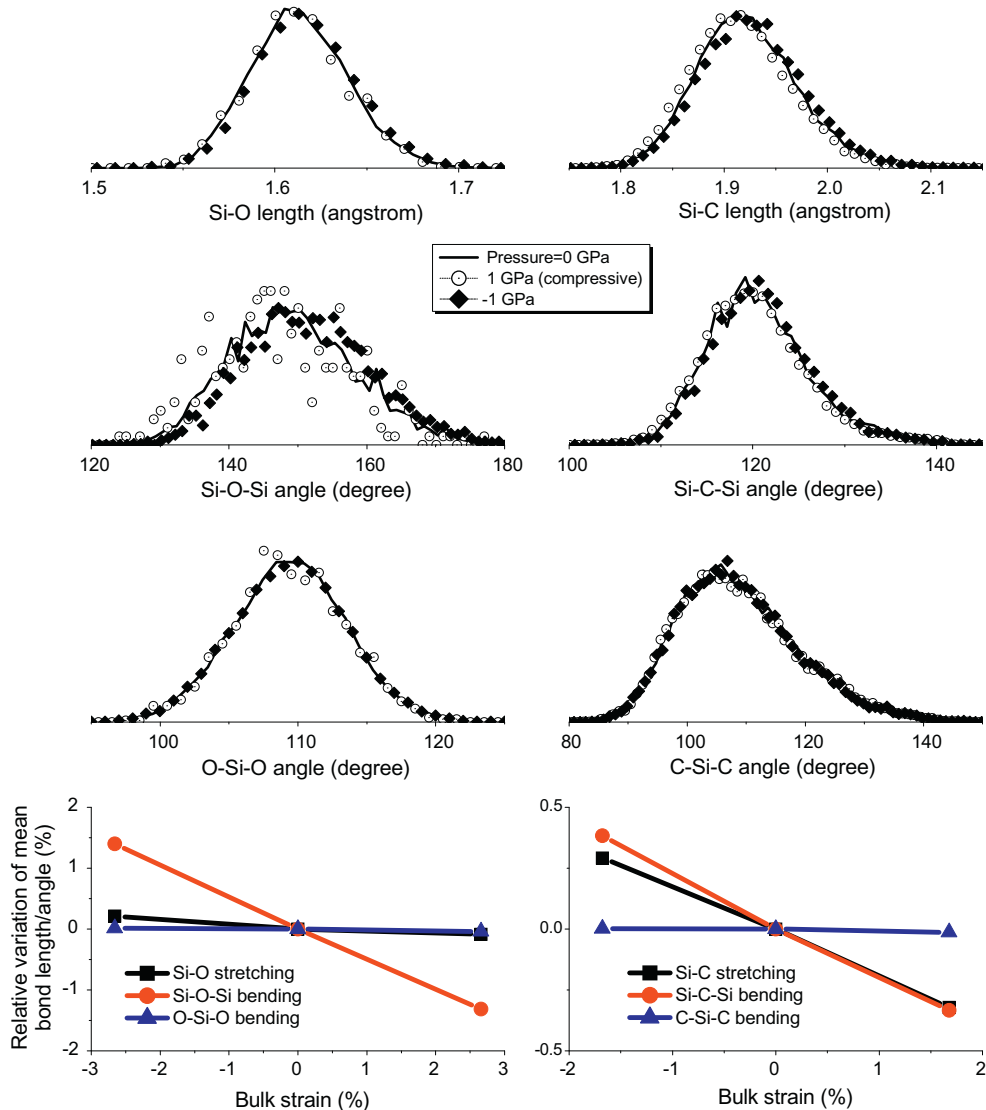


Fig. 5. Evolution of bond length and angle distribution in SiO_2 (left) and $\text{Si}(\text{CH}_2)_2$ under hydrostatic loading.

nearly unchanged. Indeed, the relative variation of the mean Si–O–Si angle per unit strain is much larger than the corresponding variation for the O–Si–O angle or the Si–O length (Fig. 5, bottom left). Thus deformation of SiO₂ under hydrostatic loading is mainly accommodated by bending of the Si–O–Si bonds connecting nearly rigid SiO₄ tetrahedra.

The SiO₂ network structure evolves rather differently under shear loading. A salient feature of this mode of deformation is that none of the bond length or angle distributions is significantly affected. More detailed information is required to describe the mechanism responsible for shear deformation, including information on (1) how individual bonds are deformed before and after shearing and (2) how the relative deformation of the bonds is distributed. As an example, Fig. 6a plots the distribution of the relative change in angle for all the Si–O–Si bonds upon shear loading, where the undeformed network was used as the reference configuration. Clearly, the distribution is symmetrical about zero angle change, i.e. the number of Si–O–Si bond angles that become larger upon shearing equals the number of Si–O–Si bond angles that decrease by the same amount. Consequently, the overall Si–O–Si angle distribution remains unchanged. This is not surprising, as shear deformation

can be decomposed into equal amounts of tensile and compressive strain along two mutually perpendicular axes. For comparison, Fig. 6b and c shows the distributions of the relative change in the Si–O–Si bond angles upon hydrostatic compression and tension, respectively. Even though the distributions are largely symmetrical, there is now a definite offset. The value of this offset is determined by the hydrostatic pressure, and is equal to the change in the mean Si–O–Si bond angle as plotted in Fig. 5. A similar analysis for all types of bonds in the network shows that bending of the Si–O–Si bonds contributes most to the shear deformation of silica. This is so because of the greater flexibility of these bonds compared with stretching of the Si–O bond or bending of the O–Si–O bond.

In Si(CH₂)₂ the Si–C–Si bond angle and the Si–C bond length distributions are much more affected by external loads (hydrostatic or shear) than the C–Si–C angle distribution. This is illustrated for hydrostatic loading in the right panels of Fig. 5. The elastic deformation of the network is accommodated primarily by bending of the Si–C–Si bonds and by stretching of the Si–C bonds. The Si–C stretching occurs in response to external loading because the Si–C–Si cross-links have a greater bending stiffness than the Si–O–Si bonds in silica. This greater bending stiffness also explains the finding that the bulk modulus of type-I OSG increases with –CH₂– population, and is consistent with the trend of our previous DFTB calculations [36]. Indeed, according to DFTB the Si–C–Si bonds have an even greater bending stiffness, thus causing a steeper rise in the network stiffness compared with the result obtained from the COMPASS force field (Fig. 4).

The differences between the MD and DFTB results, visible in Figs. 3 and 4, are mainly due to two factors: (1) the COMPASS force field allows some deformation of the Si–CH₂–Si bonds while they are nearly rigid in DFTB; (2) the DFTB calculations are static simulations at 0 K while the MD simulations are performed at finite temperature. The former effect explains the lower elastic moduli obtained for Si(CH₂)₂ in the MD simulations. The kinks in the density and modulus curves upon addition of small amounts of –CH₂– are an effect of the different thermal behavior of silica and Si(CH₂)₂, i.e. different thermal expansion coefficients and different thermal dependencies of the elastic coefficients. Considering the stiffness of Si–CH₂–Si units, it is difficult to decide which method provides a more accurate description of reality. To this end, further comparison with results from more sophisticated DFT functionals would be valuable, although we would expect the overall features to remain the same. Note that standard GGA DFT functionals tend to systematically underestimate the bulk moduli and, hence, are not suitable for use as a reference.

In summary, the MD simulation results reveal that bending of the Si–O–Si angle is the dominant deformation mechanism for a-silica, while for Si(CH₂)₂ both Si–C–Si

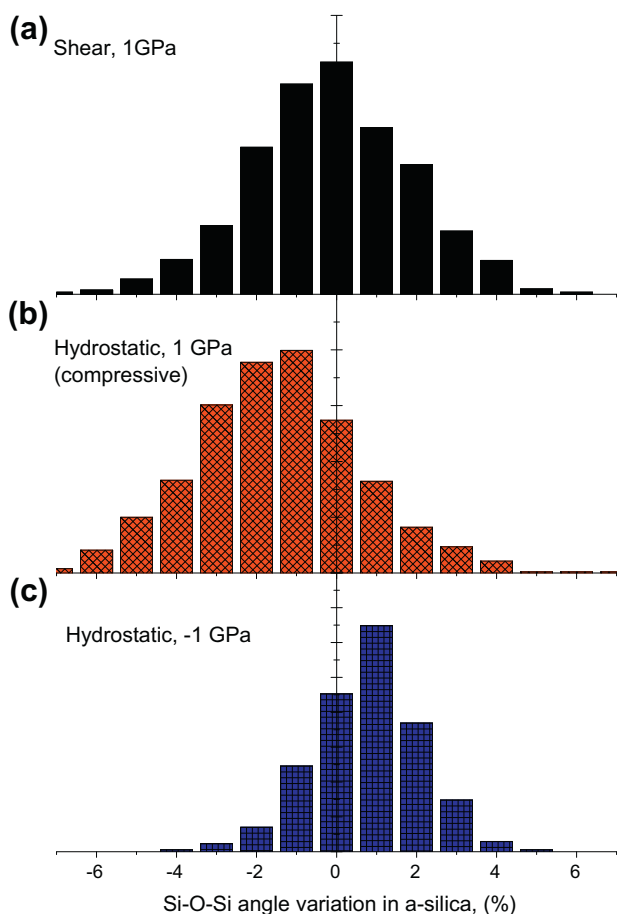


Fig. 6. Distribution of the relative changes of the Si–O–Si angles in silica under (a) a shear stress of 1 GPa, (b) hydrostatic pressures of 1 GPa (compressive) and (c) hydrostatic pressures of –1 GPa.

bond bending and Si–C stretching occur, because of the greater bending stiffness of Si–C–Si bonds compared with Si–O–Si bonds.

4.2. Type-II OSG: effect of terminal groups

Type-II OSG materials contain a number of terminal groups interrupting the network structure. Here we investigate the effects of $-\text{CH}_3$ and $-\text{OH}$ terminal groups as inspired by experiments [8,23,24]. To introduce terminal groups, a fraction of the Si–O–Si units broken and the bridging oxygen atom in each unit is replaced by two terminal groups. The disrupted network structure can be described through use of the network connectivity number $\langle r \rangle$, which is defined as the average coordination number per network-forming atom [15]. The connectivity number of type-I OSG is the same as that for a-silica ($\langle r \rangle = 2.67$), regardless of the $-\text{CH}_2-$ population. The value of $\langle r \rangle$ for type-II OSG is related to the number of terminal groups through

$$\langle r \rangle = \frac{r_{\text{Si}} \cdot N_{\text{Si}} + r_{\text{O}} \cdot N_{\text{O}} + r_{\text{T}} \cdot N_{\text{T}}}{N_{\text{Si}} + N_{\text{O}} + N_{\text{T}}} = \frac{4 \cdot N_{\text{Si}} + 2 \cdot (2N_{\text{Si}} - N_{\text{T}}/2) + N_{\text{T}}}{N_{\text{Si}} + (2N_{\text{Si}} - N_{\text{T}}/2) + N_{\text{T}}} = \frac{16}{6 + N_{\text{T}}/N_{\text{Si}}} \quad (3)$$

where $N_{\text{Si},\text{O},\text{T}}$ is the number of silicon atoms, bridging oxygen atoms or terminal groups as denoted by the subscript and $r_{\text{Si},\text{O},\text{T}}$ is the respective coordination number. Each terminal group is considered as a single atom in the calculation.

As more terminal groups are introduced the network structure is increasingly disrupted and the network connectivity $\langle r \rangle$ decreases. The MD simulations show that both the bulk modulus and the shear modulus of type-II OSG are significantly reduced (Fig. 7a), while the Poisson ratio increases (Fig. 7b). Fig. 7c further shows that the density decreases with decreasing $\langle r \rangle$ as more free volume is generated by the terminal groups. That the density of OSG decreases faster with $\langle r \rangle$ for $-\text{CH}_3$ terminal groups than for $-\text{OH}$ groups is due to the relatively larger free volume associated with the methyl group.

The trends of the elastic properties and density with $\langle r \rangle$ agree well with experimental reports in the literature on similar OSG materials [7,8,10]. In fact, it has been consistently reported by a number of researchers that UV irradiation can stabilize the OSG network through local bond rearrangement and that it can promote further development of network cross-linking by severing loose terminal groups [7,8,10]. Associated with these structural changes are a greater network connectivity, an increase in elastic modulus and in density [7,8,10] and a reduction in the Poisson ratio [10]. For a more quantitative picture, we compare our simulations with experimental results reported in the literature by several research groups [7,10,38] (see also NIST Property Data Summaries, <http://www.ceramics.nist.gov/srd/summary/SiO2.htm>). Fig. 8a plots the plane strain modulus of a range of OSG materials as a

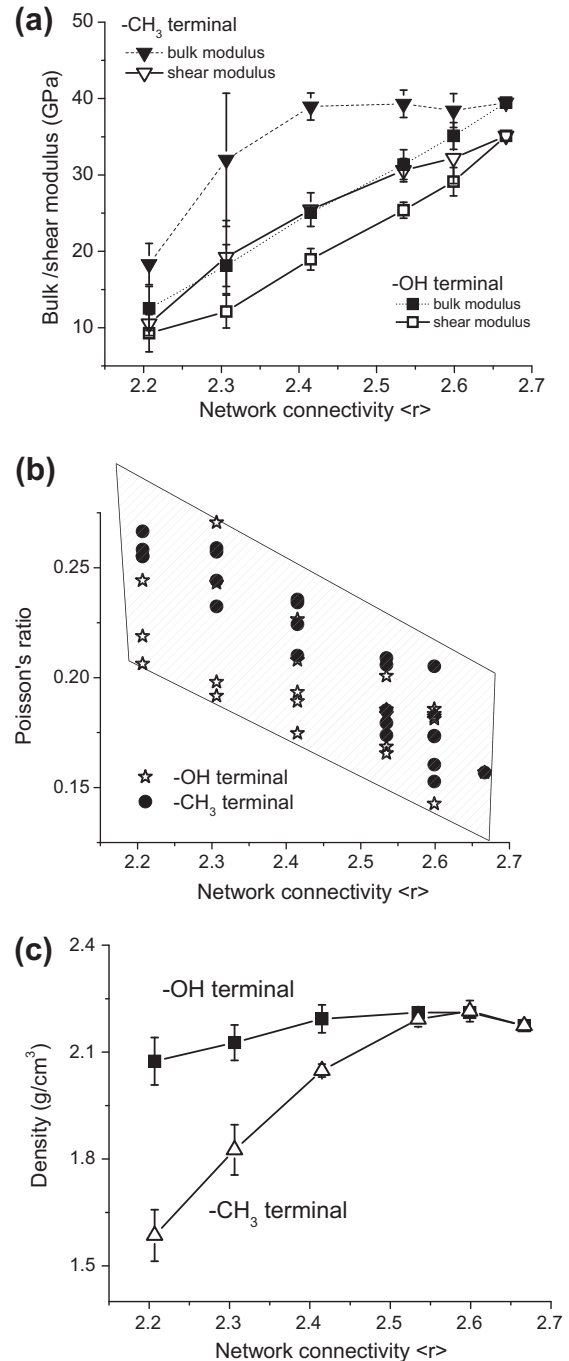


Fig. 7. (a) The bulk and shear modulus, (b) the Poisson ratio and (c) density of type-II OSG as a function of network connectivity.

function of mass density. Clearly, the MD models for type-II OSG with methyl terminal groups are in line with the experimental OSG results at the low density end and with the amorphous silica results at the high density end. Moreover, the simulation results provide a useful reference outside the material space currently accessible.

We also compare our results with MD simulations reported by Tajima et al. [20] and by Yuan et al. [39]. Tajima's OSG models are similar to ours, but these researchers allow both $-\text{CH}_3$ and $-\text{H}$ terminals at the same time. In Tajima's models the relative concentrations of the terminal

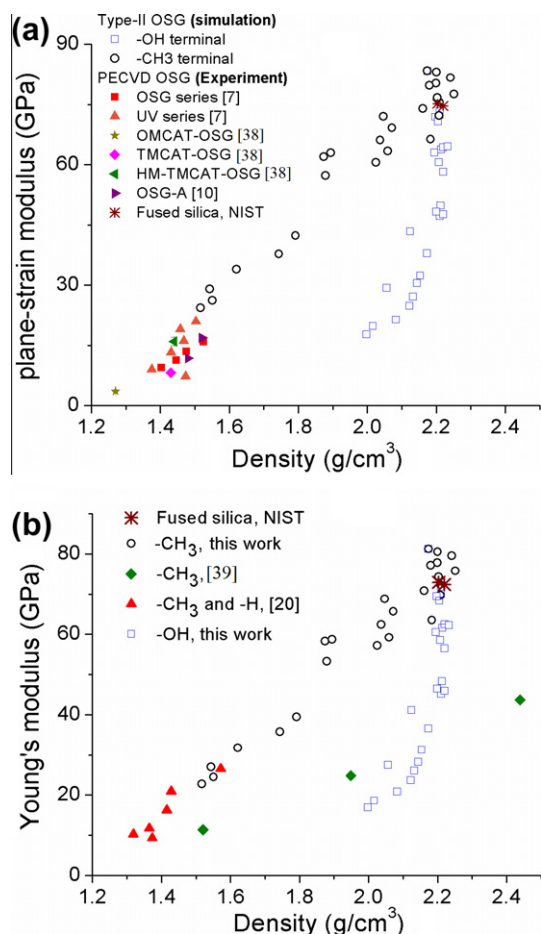


Fig. 8. (a) Plane strain modulus and (b) Young's modulus of type-II OSG as functions of density, compared with similar materials and models from (a) experimentation and (b) MD simulations, respectively.

groups are varied to best match the chemical composition and density obtained from experimental measurements and simulations are performed with the MM3 force field [40]. Yuan's model is based on a backbone framework that is initially an ordered cubic grid [39] and uses the same force field as in this study. Fig. 8b plots the Young's moduli of the material models versus density. Our results agree well with those of Tajima et al. [20,21], even though Tajima's models contain a small amount of $-H$ terminal groups and a different force field was used for the simulations. Our results differ significantly from those reported by Yuan et al. [39], probably because of the rather different method of constructing the models. More specifically, the network structure in our OSG models is similar to that of α -silica, while Yuan's model uses a network structure based on a cubic lattice. Our simulations also use periodic boundary conditions, while Yuan imposes no periodical boundary conditions.

We further compare our results with continuous random network theory. Numerical simulations based on constraint theory show that the elastic properties of a continuous random network are determined almost entirely by the network connectivity $\langle r \rangle$ [15]. Our results demonstrate that the specific terminal groups also play a significant role. For instance, Fig. 7a shows that the elastic moduli (bulk

and shear) decrease more slowly with decreasing $\langle r \rangle$ for CH_3 -terminated OSG than for OH -terminated OSG. Factors that are not included in continuous random network theory but that may be important for the stiffness of the network include: (1) the number of networking bonds per unit area, which is different for the different terminal groups; (2) long-range non-bond interactions that are different for OSG models with different terminal groups. Considering that the density of OH -terminated OSG is greater and the elastic moduli smaller than for CH_3 -terminated OSG of the same connectivity (Fig. 8a–c), we conclude that the long-range interactions are indeed important.

Another important difference between the MD simulations and constrained random network theory relates to rigidity percolation. According to classical constraint theory a network is over-constrained when the number of constraints imposed by the network bonds exceeds the degrees of freedom. If the number of constraints is smaller than the degrees of freedom, the network is under-constrained and the stiffness decreases rapidly. This transition occurs at the rigidity percolation threshold. The percolation threshold is generally not a constant but a function of the fraction of onefold coordinated atoms in the network x_1 , through $\langle r \rangle_c = 2.4 - 0.4 \cdot x_1$ [15]. For the most disrupted model in this study the percolation threshold $\langle r \rangle_c$ predicted by the random network model is 2.26. Our MD simulations, however, show that there is no sudden change in stiffness near the theoretical percolation threshold. Instead, the stiffness of the OSG networks decreases gradually over a range of $\langle r \rangle$ values. We ascribe this behavior to the long-range non-bond interactions present in the MD simulations but not considered in the continuous random network model.

4.3. Implication for the synthesis of low k dielectrics with improved rigidity

Dense OSG materials that rely on methyl groups to reduce their dielectric constants have a Young's modulus that is less than one third the modulus of silica. To further reduce the dielectric constant, porous versions of these materials have been developed and utilized in advanced integrated circuits. Unfortunately, the mechanical properties of porous dielectrics degrade rather rapidly with increasing porosity [37]. Evidently, an OSG matrix material with a high Young's modulus and low dielectric constant would make it possible to produce porous dielectrics with superior properties.

Over the past few years sol-gel synthesized oxycarbosilane organosilicates have been developed that possess improved mechanical properties over conventional organosilicates [9,11,13,14]. This is achieved by incorporating hydrocarbon groups as bridging units to increase the network connectivity over that of earlier generations of OSG. Although promising, the improved stiffness is still been far less than that of α -silica [13], presumably because of the significant number of terminal groups that are still present in the glass network.

In this study we have explored how the mass density and mechanical properties of OSG correlate with the network structure of OSG. We demonstrate that the stiffness of OSG depends not only on the network connectivity, but also on the specific bridging ligaments and terminal groups. An interesting finding is that it may be possible to fabricate OSG materials with $-\text{CH}_2-$ cross-links that are significantly stiffer than α -silica. The elastic properties of such a material are tunable by controlling the relative concentration of $-\text{CH}_2-$ cross-links versus $-\text{CH}_3$ terminal groups. Considering, for instance, the ideal case where all the bridging oxygen atoms in the silica network are replaced by $-\text{CH}_2-$ cross-links, a 50% increase in bulk modulus could be obtained over pure silica, while the density is reduced by 24%. Such a material is likely to have a low dielectric constant, as the Si–C bond is less polar than the Si–O bond [3]. Even at an intermediate and probably more realistic ratio ($\text{CH}_2/\text{Si} = 1$), a 35% modulus improvement and 6.2% density reduction can be achieved if there are no terminal groups. Using such a material as the matrix material in a porous dielectric and assuming a power law relationship between Young's modulus and porosity [37], dielectrics with a porosity of 40% would have a Young's modulus greater than 10 GPa. However, terminal groups always exist in real materials. They are responsible for decreased network connectivity and a rapid loss of mechanical integrity. To attain optimum electrical and mechanical properties, further development of the synthesis chemistry and remedial treatments is required to minimize the terminal group population.

5. Conclusions

We have used MD simulations to investigate the fundamental structure–property relationships of organosilicates with a primary focus on the mass density and elastic properties of the material. By examining two representative classes of material models the strengthening effects of incorporating organic cross-links in the glass network and the detrimental effects of terminal groups are modeled and discussed. Quantitative guidelines are attained for the bottom-up design of new organosilicate materials with a high modulus and low dielectric constant.

Acknowledgements

H.L. and J.J.V. acknowledge support from the National Science Foundation under Grant DMR-0906892. J.M.K. is grateful for a scholarship grant from the German Research Association. Assistance in part of the simulation work by Arjan Mundy is also gratefully acknowledged. We would like to thank X. Chen for help with the MD simulation software.

References

[1] Grill A, Patel V. *Appl Phys Lett* 2001;79(6):803.

- [2] Morgen M, Ryan ET, Zhao JH, Hu C, et al. *Annu Rev Mater Sci* 2000;30:645.
- [3] Maex K, Baklanov MR, Shamiryan D, Iacopi F, et al. *J Appl Phys* 2003;93(11):8793.
- [4] Grill A, Edelstein D, Restaino D, Lane M, et al. In: *Interconnect technology conference*. Burlingame, CA: IEEE; 2004.
- [5] McGahay V, Bonilla G, Chen F, Christiansen C, et al. In: *Interconnect technology conference*. Burlingame, CA: IEEE; 2006.
- [6] Thorpe MF. *J Non-Cryst Solids* 1983;57(3):355.
- [7] Youbo Lin, Yong Xiang, Tsui Ting Y, Vlassak JJ. *Acta Mater* 2008;56(17):4932.
- [8] Iacopi F, Travaly Y, Eyckens B, Waldfried C, et al. *J Appl Phys* 2006;99(5):053511.
- [9] Dubois G, Volksen W, Magbitang T, Miller RD, et al. *Adv Mater* 2007;19(22):3989.
- [10] Iacopi F, Beyer G, Travaly Y, Waldfried C, et al. *Acta Mater* 2007;55(4):1407.
- [11] Kim S, Toivola Y, Cook RF, Char K, et al. *J Electrochem Soc* 2004;151(3):F37.
- [12] Gage DM, Stebbins JF, Peng LM, Cui ZJ, et al. *J Appl Phys* 2008;104(4):043513.
- [13] Rathore JS, Interrante LV, Dubois G. *Adv Funct Mater* 2008;18(24):4022.
- [14] Dubois G, Volksen W, Magbitang T, Sherwood MH, et al. *J Sol–Gel Sci Technol* 2008;48(1/2):187.
- [15] He H, Thorpe MF. *Phys Rev Lett* 1985;54(19):2107–10.
- [16] Bazant MZ, Kaxiras E, Justo JF. *Phys Rev B* 1997;56(14):8542.
- [17] Van Ginhoven RM, Jonsson H, Corrales LR. *Phys Rev B* 2005;71(2):024208.
- [18] Guttman L, Rahman SM. *Phys Rev B* 1988;37(5):2657.
- [19] Tajima N, Ohno T, Hamada T, Yoneda K, et al. *Jpn J Appl Phys, Part 1* 2007;46(9A):5970.
- [20] Tajima N, Ohno T, Hamada T, Yoneda K, et al. *Appl Phys Lett* 2006;89(6):061907.
- [21] Tajima N, Hamada T, Ohno T, Yoneda K, et al. In: *Proceedings of IEEE international interconnect technology conference, 2005*. San Francisco, CA: IEEE; 2005. p. 66–8.
- [22] Choi Hyuk Soon, Lee Taebum, Lee Hyosug, Kim Jongeseob, et al. In: *Materials research society '05 fall meeting*. Boston (MA): Materials Research Society; 2005.
- [23] Grill A, Neumayer DA. *J Appl Phys* 2003;94(10):6697.
- [24] Lin YB, Tsui TY, Vlassak JJ. *J Electrochem Soc* 2006;153(7):F144.
- [25] Sun H. *J Phys Chem B* 1998;102(38):7338.
- [26] Huff NT, Demiralp E, Cagin T, Goddard WA. *J Non-Cryst Solids* 1999;253:133.
- [27] Andersen HC. *J Chem Phys* 1980;72(4):2384.
- [28] Parrinello M, Rahman A. *J Appl Phys* 1981;52(12):7182.
- [29] Weiner JH. *Statistical mechanics of elasticity*. New York: John Wiley; 1983.
- [30] Ewald PP. *Ann Phys* 1921;64(3):253.
- [31] Verlet L. *Phys Rev* 1967;159(1):98.
- [32] Accelrys Inc. *Materials Studio R4.0*. San Diego, CA, USA.
- [33] Mauri F, Pasquarello A, Pfommer BG, Yoon YG, et al. *Phys Rev B* 2000;62(8):R4786.
- [34] Mozzi RL, Warren BE. *J Appl Crystallogr* 1969;2:164.
- [35] Neuefeind J, Liss KD. *Ber Bunsen-Ges Phys Chem* 1996;100(8):1341.
- [36] Knaup JM, Li H, Vlassak JJ, Kaxiras E. In: *Bauer AJ, Friedrichs P, Krieger M, Pensl G, Rupp R, Seyller T, editors. Silicon carbide and related materials 2009*. Stafa-Zurich, Switzerland: Trans Tech Publications; 2010. p. 267–70.
- [37] Li H, Lin Y, Tsui TY, Vlassak J. *J Mater Res* 2009;24(1):107.
- [38] Tsui TY, Griffin AJ, Fields R, Jacques JM, et al. *Thin Solid Films* 2006;515(4):2257.
- [39] Yuan CA, van der Sluis O, Zhang GQ, Ernst LJ, et al. *Comput Mater Sci* 2008;42(4):606.
- [40] Allinger NL, Yuh YH, Lii JH. *J Am Chem Soc* 1989;111(23):8551.